Study on the Thermohydraulic Performance of Double Pass Solar Air Heater

Ankush Hedau* and S. K. Singal

Department of Hydro and Renewable Energy, Indian Institute of Technology Roorkee (India)

*Corresponding author: ankush.hedau@gmail.com

Abstract

Experimental and numerical investigations are conducted in this study to optimize different turbulence models and thermohydraulic performance of double pass solar air heater (DPSAH) under different Reynolds numbers (*Re*) of 3000 to 19000. The DPSAH was investigated using five different turbulence models: SST-k-ω, standard k-ω, realizable k-ε, RNG k-ε, and standard k-ε. Using the RNG k-ε turbulence model, the experimental results are found in close agreement with the numerical results, with an average absolute deviation of 2.6% for the Nusselt number (*Nu*) and an average absolute deviation of 0.4% for friction factor (*f*). In comparison to single pass solar air heater (SPSAH), the DPSAH enhanced the values of the Nusselt number (*Nu*) from 1.13 to 1.89 and increased the values of friction factor (*f*) from 2.69 to 3.5 for a considered range of *Re*. The maximum thermohydraulic performance parameter (THPP) over the SPSAH was obtained as 1.25, which corresponds to *Re* of 19000.

Keywords: Thermohydraulic performance, solar energy, computational fluid dynamics, friction factor, Nusselt number

1. Introduction

Energy consumption is increasing day by day throughout the world due to rising population, technological advancements, and economic developments. Moreover, the major portion of energy consumption is met by the non-renewable sources of energy such as coal, natural gas and petroleum oil, causing an increase the global warming and greenhouse gas emissions. It is essential to utilize renewable energy sources (solar energy, biomass energy, geothermal energy, and wind energy) in order to reduce the impact of global warming and greenhouse gas emissions. Solar energy is found to be the highest potential renewable energy source that fulfils the world's energy requirement. Solar air heater (SAH) is a device which harnesses solar energy for a wide range of low-temperature purposes, including drying, natural ventilation and greenhouse heating. There are two primary components of the SAH. These two components are the absorb plate and the glass cover. As a heat transfer medium, the SAH utilizes air to transfer heat.

In SAH, the main drawback is the low heat transfer between the absorber plate and the air. This is because of the thermal boundary layer formation along the length of the absorber plate. In order to increase the heat transfer, the absorber plate's surface area must be increased in contact with the air. Further, the SAH is categorized according to the number of passages as either double pass or single pass. Moreover, SAH with double pass is more effective than SAH with a single pass due to its large heat contact surface area (Hernández and Quiñonez 2013; Kabeel et al. 2017). The various authors conducted experimental and numerical investigations on the double pass solar air heater (DPSAH) and single pass solar air heater (SPSAH), which are discussed in the following paragraphs.

An extensive literature review was presented by Alam and Kim (2017) on different methods of improving the performance of a DPSAH. The results concluded that the performance was enhanced with DPSAH because of increased heat transfer surface area, turbulence intensity, and reduced thermal losses. The thermal performance of DPSAH was found to be greater than that of SPSAH. The comparative analysis of the SPSAH and DPSAH filled with porous media in the lower passage was experimentally presented by Kareem et al. (2013). It was observed that the thermal performance of SAH increases with increasing number of passes. The maximum

10.18086/swc.2023.04.07 Available at http://proceedings.ises.org

thermal efficiency of the SPSAH and DPSAH was achieved to be 52% and 70 %, respectively. Hernández and Quiñonez (2013) examined the thermal behaviour of parallel and counter-flow DPSAH. They developed various mathematical expressions to evaluate the heat transfer coefficients and heat transfer removal factor of the SAHs. The double pass counter flow had higher temperature rise compared to double pass parallel flow.

Gill et al. (2012) studied the thermal performance of single-glazed and double-glazed SAHs. It is seen that double-glazed SAH has higher stagnation temperatures and thermal efficiency. The double-glazed SAH is more cost-effective in terms of air outlet temperatures and thermal efficiency than a single-glazed SAH. The thermal performance of SPSAHs was numerically analyzed by Yadav and Bhogoria (2013) using five different turbulence models: SST-k-ω, standard k-ω, realizable k-ε, RNG k-ε, and standard k-ε. The RNG k-ε turbulence proved the best turbulence model to validate with the Dittus-Boelter equation and Blassius equation. Kumar (2017) numerically analyzed the thermohydraulic performance of V-corrugated SAHs with an RNG k-ε turbulence model. It was concluded that V corrugated SAH has better thermohydraulic performance than smooth flat plate SAHs.

From an extensive literature review, it has been concluded that counter-flow DPSAHs have better outlet temperatures and thermal efficiency than SPSAHs. However, no study has been conducted on a DPSAH with different turbulence model. The thermohydraulic performance of DPSAHs has not yet been reported. Accordingly, an experimental and numerical investigation is conducted in order to examine the thermohydraulic performance of DPSAH having five different turbulence models (SST-k-ω, standard k-ω, realizable k-ε, RNG k-ε, and standard k-ε).

2. Numerical approach

Computational fluid dynamics (CFD) is a method of analyzing fluid flow and heat transfer in DPSAHs. In the present study, the numerical analysis is conducted on DPSAH with ANSYS Fluent 2020 R_2. The numerical approach is explained in the following subsections.

2.1. Computational model

ANSYS design modeler was used to develop the computational model of DPSAH, which has dimensions of 35 mm height, 1000 mm length, and 350 mm width. The computational domain consists of lower and upper passages, each with a height of 35 mm. However, 50 mm air circulation gap was provided near the U-turn passage to divert air from the lower passageway to upper passageway and to minimize the pressure loss. The dimension of computational domain is shown in Fig. 1.

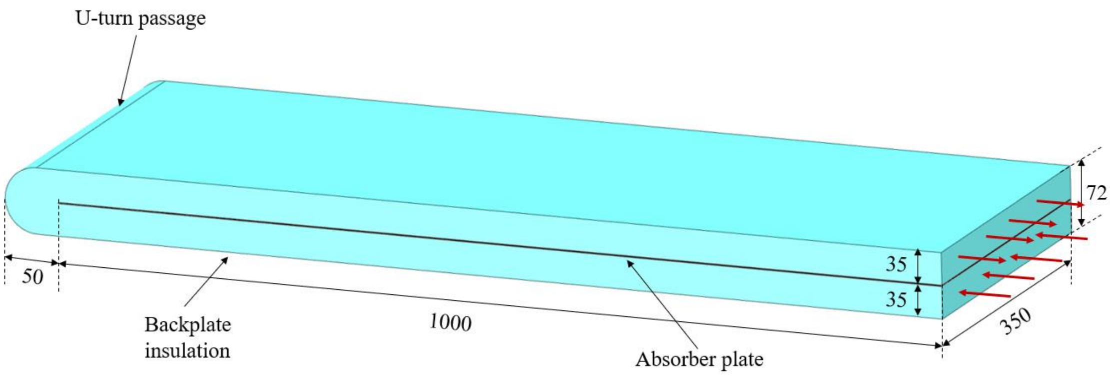

Fig. 1: Three-dimensional computational domain of double pass solar air heater (DPSAH) (All dimensions are in mm)

Assumptions considered during CFD analysis: (i) Flow is steady, incompressible, 3-dimensional, turbulent and fully developed (ii) The air outlet pressure should equal the gauge pressure (iii) The properties of the absorbing plate and air are kept constant (iv) Heat transfer due to radiation is negligible as solar radiation of 880 Wm^{-2} is uniformly distributed across the absorber plate (v)The sidewall and bottom plate are considered insulated.

2.2. Meshing

Heat transfer and fluid flow were analyzed by dividing the computational model into number of elements and cells using a grid generation method. The meshing of DPSAH is shown in Fig. 2. A uniform and fine grid was created with the meshing module in Ansys 2020 R_2. The smoothing was high for creating a uniform grid. Fine and uniform meshing were used for accurate flow simulation. Grid-independence test (GIT) was performed with an RNG k-ε turbulence model to accommodate small deviation in friction factor (*f*) and Nusselt number (*Nu*). The elements varied between 369026 and 3959280 for Reynolds number (*Re*) of 5000, as shown in Tab. 1. The number of elements increased until *Nu* and *f* deviations were less than 1%. The optimum number of nodes and elements for the grid independence test were found to be 2488827 and 2300638, respectively.

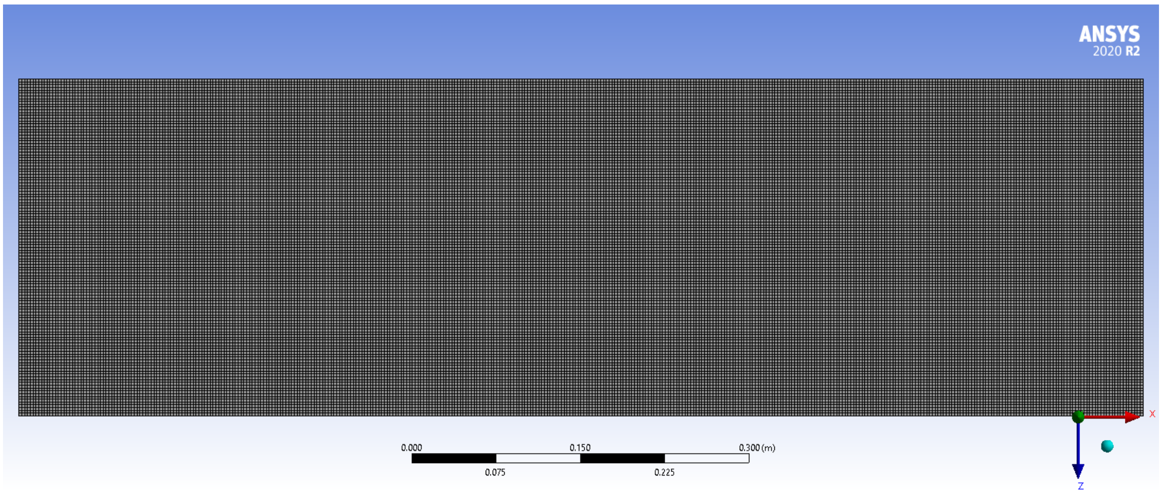

Fig. 2: Meshing of the absorber plate of DPSAH.

Tab. 1: Grid independence test of DPSAH for *Re* of 5000

Element size	**No. of nodes**	**No. of elements**	***Nu***	***f***	**% Variations in *Nu***	**% Variations in *f***
0.0035	425169	369026	18.34	0.0327		
0.003	684982	608800	19.37	0.0321	5.32	1.97
0.0027	863500	771502	20.20	0.0323	4.11	0.54
0.0024	1283028	1166286	20.92	0.0320	3.44	0.87
0.0021	1895184	1739881	21.69	0.0323	2.55	0.84
0.0019	2488827	2300638	21.90	0.0321	0.96	0.58
0.0018	2951088	2740804	22.11	0.0320	0.95	0.26
0.0017	3503538	3268496	22.31	0.0318	0.90	0.56

2.3. Governing equation

To analyze the fluid flow and heat transfer of DPSAH, three governing equations, namely the energy equation, continuity equation and Navier-Stokes equation, were applied. The finite volume method (FVM) solves these governing equations for steady-state regimes. This system was governed by the following 3D equations in Cartesian coordinates:

Continuity equation (Mass conservation equation)

$$\frac{\partial(\rho u_j)}{\partial x_j} = 0 \qquad \text{(eq. 1)}$$

Navier-Stokes equation (Momentum conservation equation)

$$\frac{\partial}{\partial x_i}(\rho u_i u_j) = -\frac{\partial P}{\partial x_i} + \frac{\partial}{\partial x_j}\left[\mu\left(\frac{\partial(\rho u_i)}{\partial x_i} + \frac{\partial(\rho u_j)}{\partial x_j}\right)\right] + \frac{\partial}{\partial x_j}\left[-\overline{\rho u'_i u'_j}\right] \qquad \text{(eq. 2)}$$

Energy conservation equation

$$\frac{\partial}{\partial x_i}\left(\rho u_j T\right) - \frac{\partial}{\partial x_j}\left[\left(\Gamma + \Gamma_t\right)\frac{\partial T}{\partial x_j}\right] = 0 \quad \text{(eq. 3)}$$

The governing equations were solved in the present study with the help of boundary conditions mentioned in Tab. 2.

Tab. 2. Boundary conditions

Boundary zone	Zone condition	Zone type	Values
Inlet	Velocity inlets	Fully developed	1.23 to 4.67 ms^{-1} (3000 to 19000)
Outlet	Pressure outlets	Fully developed	101.3 kPa (Atm.)
Absorber plate	Wall	No slip	880 Wm^{-2}
Side and bottom wall	Wall	No slip	Insulated

2.4. Turbulence model and solution method

The double-precision pressure-based solver was used for predicting accurate flow simulations. A least square-based method was used to perform the spatial discretization. To simulate fluid flow and heat transfer behaviour, second-order upwind scheme was used to account for continuity, pressure, momentum, turbulence dissipation rate, turbulent kinetic energy and energy equation. The SIMPLE algorithm was selected for solving governing equations based on the conservation laws and boundary conditions. The convergence criteria selected for continuity equation was 10^{-3}, and for the momentum and energy equation was 10^{-6}. The numerical investigation of DPSAH was carried out on five different turbulence models such as realizable k-ε, RNG k-ε, standard k-ε, SST-k-ω and standard k-ω turbulence model.

In order to validate the turbulence model of DPSAH, the experimental testing rig is designed and manufactured, which is discussed in the next section.

3. Experimental Study

3.1. Details of the experimental approach

The experimental testing rig consists of four parts: rectangular duct, solar simulator, data acquisition system and air circulating unit, as illustrated in Fig. 3.

The solar simulator was designed and manufactured with dimensions of 1600 mm×400 mm and consists of 24 halogen tubes, four dimmers, and an iron frame. The solar simulator was powered by variac to produce solar radiation of 1000 Wm^{-2}. The solarimeter measures the intensity of solar radiation in order to maintain a uniform solar radiation of 1000 Wm^{-2} throughout the glass cover.

There are three sections along the length of air duct: the entry section, the test section and the exit section. For the flow to be fully developed inside the duct, the entry and exit sections were kept at 550mm in length, as per the ASHRAE standard (Standard 1986). To increase the absorption of incoming solar radiations, aluminium was used as the absorbing plate, which was covered with a black paint coat. A lower passage of 35 mm was provided between the backplate and absorber plate, and upper passage of 35 mm between the absorber plate and glass cover. The glass cover thickness of 4 mm, having transmissivity of 0.88 and absorptivity of 0.1, was used.

To reduce the conduction and convective losses to the atmosphere, three different insulation materials were provided at the sidewalls and bottom wall of the rectangular duct. The first insulation layer was provided by the plywood thickness of 12 mm to reduce the conduction losses. The plywood was covered by glass wool of thickness of 6 mm. The glass wool was covered by thermocol with thickness of 12 mm to minimize the heat losses to the surroundings. The centrifugal blower powered by a motor rating of 2 kW,230V running at 2880 rpm was used to suck the air from the atmosphere and direct the air from the lower passageway to upper passageway.

The 52 T-type thermocouples were calibrated by Fluke 9142. With the help of two data loggers (midi LOGGER GL800), temperature data was recorded from thermocouples attached to the inlet and outlet sections, as well as the heating surface of the absorber plate. The U-tube manometer and the orifice plate were used for measuring the mass flow rate of the air, and the control valve was used for controlling the mass flow rate of the air. The digital manometer was used to measure the pressure difference of the rectangular duct.

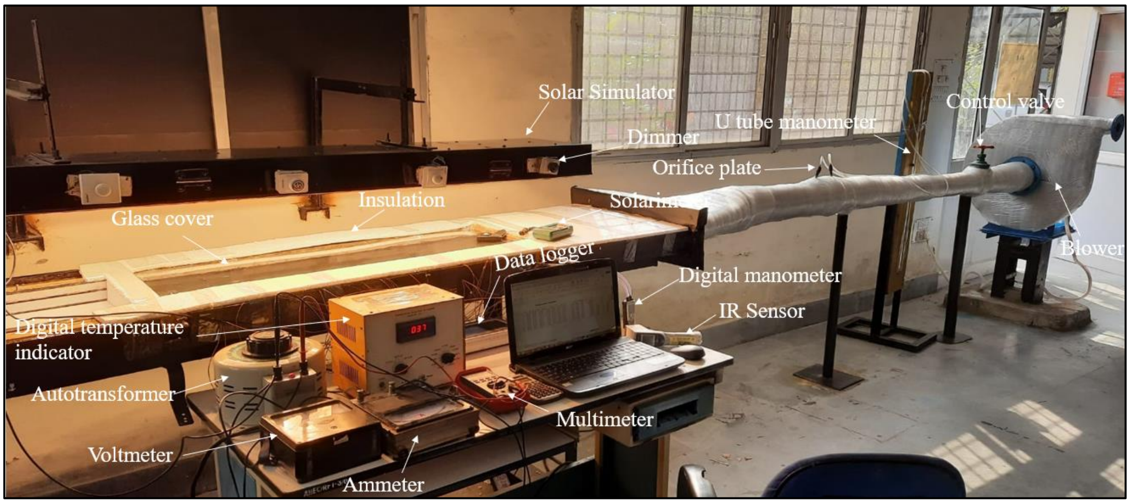

Fig. 3: Experimental test rig of DPSAH

3.2. Data collection

The following parameters were recorded under the steady state conditions.

- Pressure difference across the orifice plate (ΔP).
- Lower and upper absorber plate temperatures (T_{pm})
- Temperatures of inlet air (T_{in}) were recorded at inlet of the lower passage.
- Temperatures of the outlet air (T_{out}) were recorded at outlet of the upper passage.
- Pressure difference inside the duct $(\Delta P)_d$.

The various mathematical formulations were used to calculate the values of friction factor (f), Nusselt number (Nu), and THPP of DPSAH, which are discussed in the following subsections.

3.3. Data reduction

Using the value of pressure difference across the orifice plate (ΔP), airflow inside duct is calculated as follows:

$$\dot{m} = C_d \times A_o \times \left[\frac{2 \times \rho_a \times (\Delta P)}{1 - \beta^4}\right]^{0.5} \qquad \text{(eq. 4)}$$

Where C_d is the orifice plate discharge coefficient, A_o is the orifice area, and β is the ratio of the orifice meter radius to orifice pipe the radius.

The air velocity (V) is calculated as follows:

$$V = \frac{\dot{m}}{\rho_a \times W \times H} \qquad \text{(eq. 5)}$$

The value of Re is determined as follows:

$$Re = \frac{\rho_a \times V \times D_h}{\mu} \qquad \text{(eq. 6)}$$

Where D_h represent equivalent diameter and is calculated as:

$$D_h = \frac{4\,(W \times H)}{2\,(W + H)} \qquad \text{(eq. 7)}$$

The air heat gain (Q_u) is mathematically determined as follows:

$$Q_u = \dot{m} \times C_{pa} \times (T_{out} - T_{in}) \quad \text{(eq. 8)}$$

The convective coefficient (h) is determined by equating value of Q_u to the convective heat transfer rate (Q_{conv}), as follows.

$$h = \frac{Q_u}{A_p(T_{pm} - T_{am})} \quad \text{(eq. 9)}$$

T_{pm} and T_{am} are the mean weighted average temperature of the absorber plate and air, respectively.

The value of Nu is determined as follows (Kays 1985).

$$Nu = \frac{h \times D_h}{k} \quad \text{(eq. 10)}$$

The value of f is determined as follows (Brown 2002).

$$f = \frac{(\Delta P)_d D_h}{2\rho_a L V^2} \quad \text{(eq. 11)}$$

Using the thermohydraulic performance parameter (THPP), the optimal value of DPSAH is determined as follows (Webb and Eckert 1972).

$$\text{THPP} = \left(\frac{Nu}{Nu_s}\right) \Big/ \left(\frac{f}{f_s}\right)^{1/3} \quad \text{(eq. 12)}$$

3.4. Validation of experimental results

The experimental setup was designed and constructed to determine the accuracy of the experimental results of SPSAH. The values of Nu_s and f_s of SPSAH were validated with the Dittus-Boelter and Blasius equations, respectively. The Dittus-Boelter equation and Blasius equation correlations are expressed as follows.

Dittus-Boelter correlation (Kays 1985),

$$Nu_s = 0.023(Re)^{4/5}\,(Pr)^{0.4} \quad \text{(eq. 13)}$$

Blasius correlation (BHATTI 1987),

$$f_s = 0.085(Re)^{-\frac{1}{4}} \quad \text{(eq. 14)}$$

The experimental validation of Nusselt number (Nu_s) and friction factor (f_s) with empirical correlations is shown in Fig. 4. It is seen that the experimental results of SPSAH are found to be in good agreement with the empirical correlations developed for the value of Nu_s and f_s. The mean absolute percentage error was found as 1.4% for the value of Nu_s and 6.8% for the value of f_s.

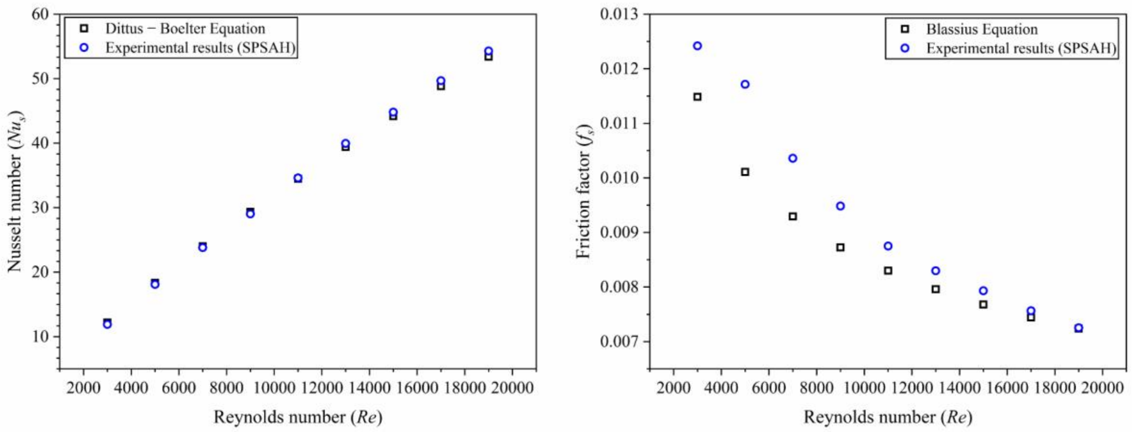

Fig. 4: Experimental validation of the Nu_s and f_s for the single pass solar air heater (SPSAH)

In order to optimize the turbulence models for the DPSAH, an experimental setup was developed following the experimental validation of SPSAH. The thermohydraulic performance parameter is further analyzed in comparison with the SPSAH.

4. Result and Discussions

In the present study, the optimization of different turbulence models and thermohydraulic performance of DPSAH is carried out for *Re* varied from 3000 to 19000 and is discussed below sub-sections.

4.1. Optimization of turbulence model of DPSAH.

The numerical results of smooth plate DPSAH with different turbulence models are compared to the experimental results for the values of *Nu* and *f*. The optimization of turbulence models is carried out for the value of *Re* from 3000 to 19000.

The variation in *Nu* with *Re* for different turbulence models and experimental results is presented in Fig. 5. It is found that the RNG k-ε turbulence model with enhanced wall treatment gives the least mean absolute percentage error (MAPE) of 2.6 % in *Nu* for the range of *Re* considered. This is due to the RNG k-ε turbulence model predicts the average absorber plate temperature to be close to the experimental results, as shown in Tab. 3. The static temperature contours corresponding to the different turbulence model at *Re* of 7000 are shown in Fig. 6. From the temperature contours, it can be concluded that the RNG k-ε model exhibits almost the same temperature distribution as the realizable K-e and standard k-ε models. Moreover, the realizable k-ε turbulence model and standard K-e turbulence model with enhanced wall treatment have more deviation in *Nu* at a low value of *Re*, and deviation has decreased with an increase in *Re*, and the corresponding MAPE is found as 4.1% and 4.8%, respectively. The k-ε turbulence model gives the closest results to the experimental results because it considers two more transport equation: turbulence dissipation rate (ε) and kinetic energy (k).

In comparison to experimental results, the standard k-ω turbulence model and SST- k-ω turbulence model gives more deviation in *Nu* at a low value of *Re*, and the deviation increases as the value of *Re* increases. The corresponding MAPE is found to be 8.6% and 11%, respectively. The reason for this is that k-ω predicts an absorber plate temperature that is higher than the experimental results, resulting in a large deviation in *Nu*.

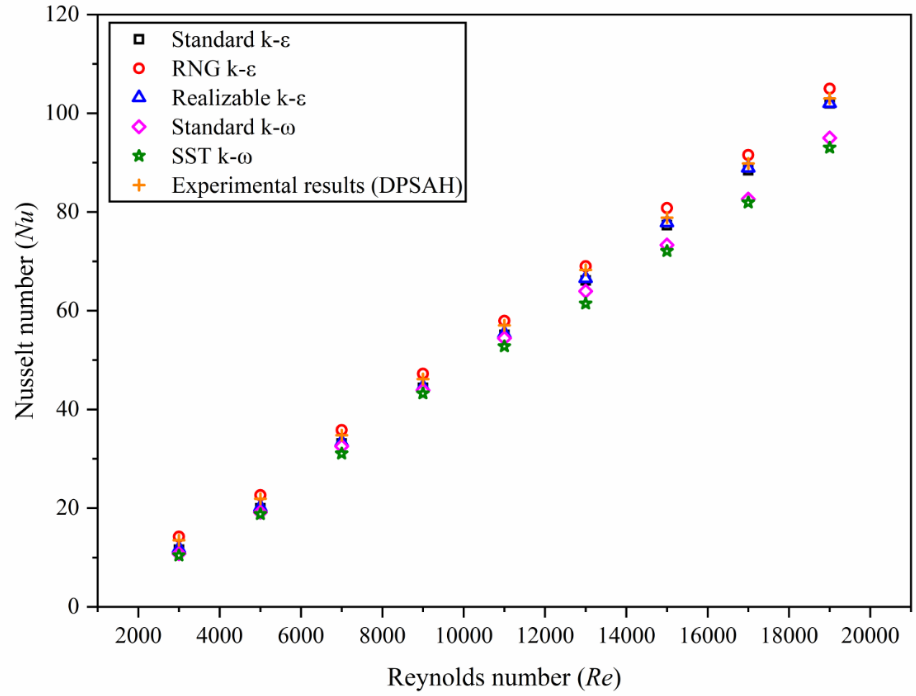

Fig. 5: Variation of *Nu* with *Re* of DPSAH with different turbulence models

Tab. 3: Average absorber temperature (T_{pm}) corresponding to the different turbulence models.

Turbulence model	Standard k-ε	RNG k-ε	Realizable k-ε	Standard k-ω	SST- k-ω	Experimental Results
T_{pm} (K) at Re=3000	397.88	393.57	395.98	398.51	398.70	390.52
T_{pm} (K) at Re=5000	377.09	374.18	376.88	379.01	379.00	370.75
T_{pm} (K) at Re=7000	360.28	358.35	360.12	361.28	362.34	354.95
T_{pm} (K) at Re=9000	350.70	349.16	350.64	351.03	351.83	345.88
T_{pm} (K) at Re=11000	343.90	342.65	343.82	344.73	345.22	339.35
T_{pm} (K) at Re=13000	338.65	337.60	338.54	339.62	340.53	334.15
T_{pm} (K) at Re=15000	334.57	333.56	334.43	335.85	336.24	330.34
T_{pm} (K) at Re=17000	331.24	330.48	331.11	332.70	332.81	327.11
T_{pm} (K) at Re=19000	328.54	327.97	328.47	329.01	330.39	324.55

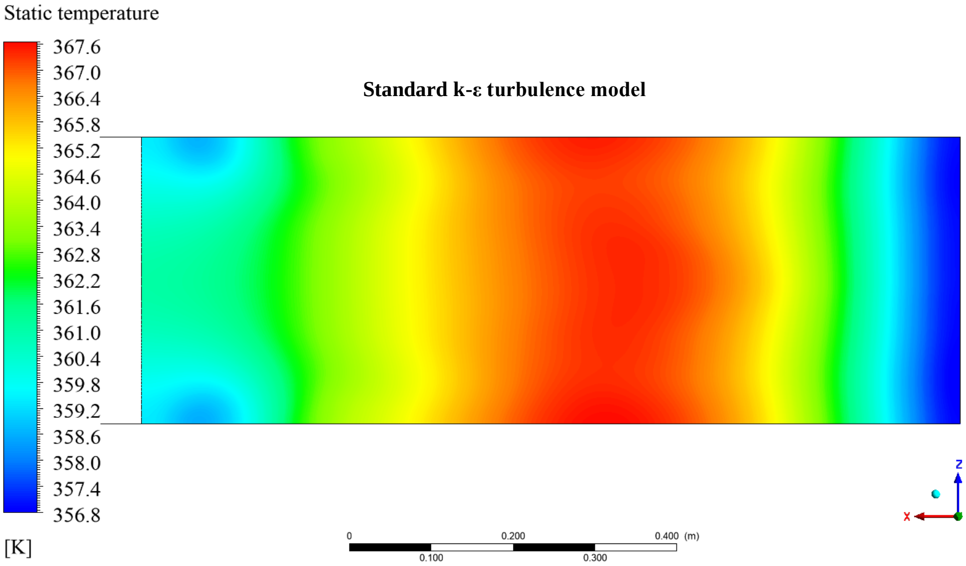

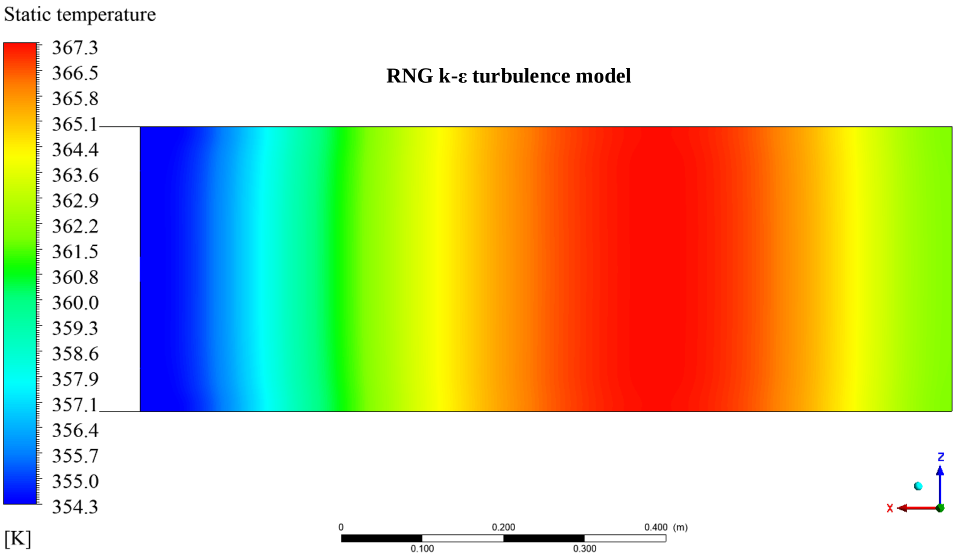

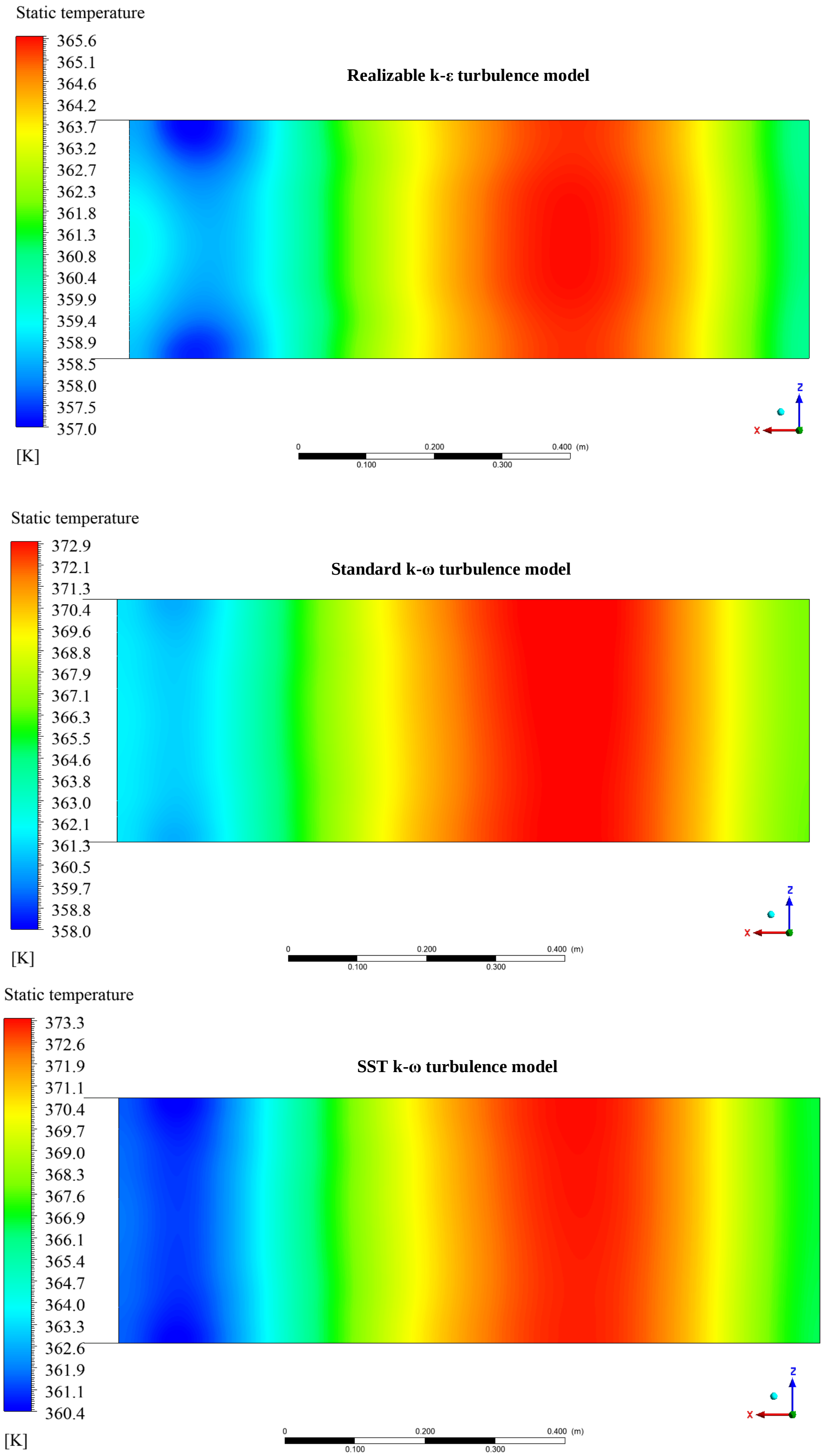

Fig. 6: Static temperature contours corresponding to the different turbulence model at *Re* of 7000

The variation in *f* with *Re* for different turbulence models and experimental results is presented in Fig. 7. For the considered range of *Re*, the RNG k-ε turbulence model with enhanced wall treatment is found in close agreement to experimental results with MAPE of 0.4%. Furthermore, the standard k-ω model, SST- k-ω model, standard k-ε model and realizable k-ε model are also validated with experimental results with MAPE of 0.8%, 2%, 2.1% and 3.9%, respectively. The results showed that the friction factor (*f*) accuracy is much better than the Nusselt number (*Nu*). The reason is that the values of *Nu* deal with various factors, such as uncertainties in the boundary conditions, heat transfer mechanisms, or inherent complexities within the system. In contrast, the friction factor (*f*) of a rectangular duct depends only on flow behaviour.

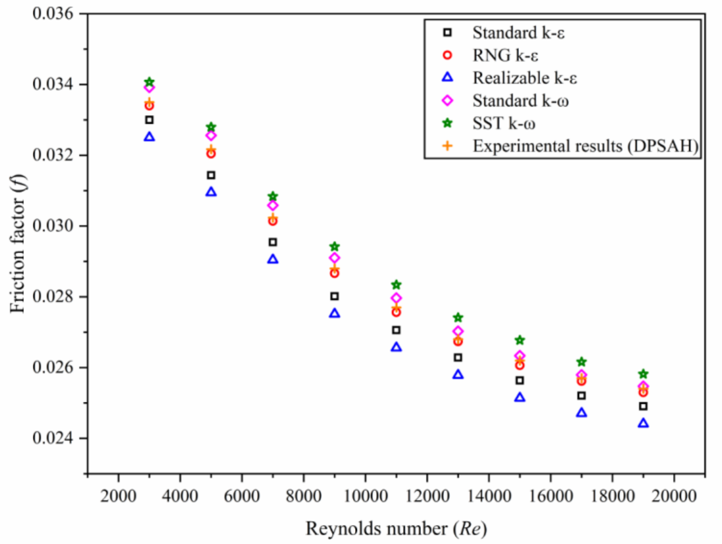

Fig. 7. Variation in *f* with *Re* of the DPSAH under different turbulence models

4.2. Thermohydraulic performance

The variation of friction factor increment (f/f_s), Nusselt number enhancement (Nu/Nu_s), and THPP with *Re* of a DPSAH is shown in Fig. 8. It is found that the values of *f/fs*, Nu/Nu_s, and THPP increase with increasing value of *Re*. Compared to SPSAH, the DPSAH increased Nu/Nu_s from 1.13 to 1.89 and f/f_s from 2.69 to 3.5 over the range of *Re*. The thermo-hydraulic performance parameter (THPP), as defined in eq. 12, is used to determine the optimum performance of DPSAH. The results showed that the THPP is less than 1 for values of *Re* below 6500, which is not advantageous. It is due to the high value of f/f_s in comparison to Nu/Nu_s. Further, with an increase in *Re* from 6500 to 19000, the THPP value also increases. This happens because heat contact surface area increases with increasing values of *Re*. As a result, the outlet temperature of the DPSAH is increased over that of the SPSAH, thereby increasing the effective heat gain and the THPP, as shown in Fig. 9. The maximum value of the THPP over the SPSAH was determined as 1.25, which corresponds to *Re* of 19000.

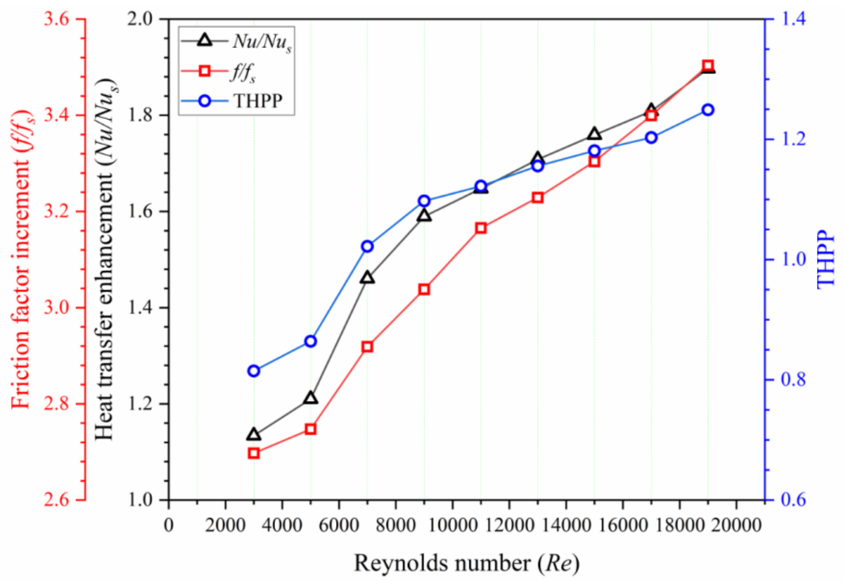

Fig. 8: Variation of Nu/Nu_s, f/f_s and THPP with *Re*

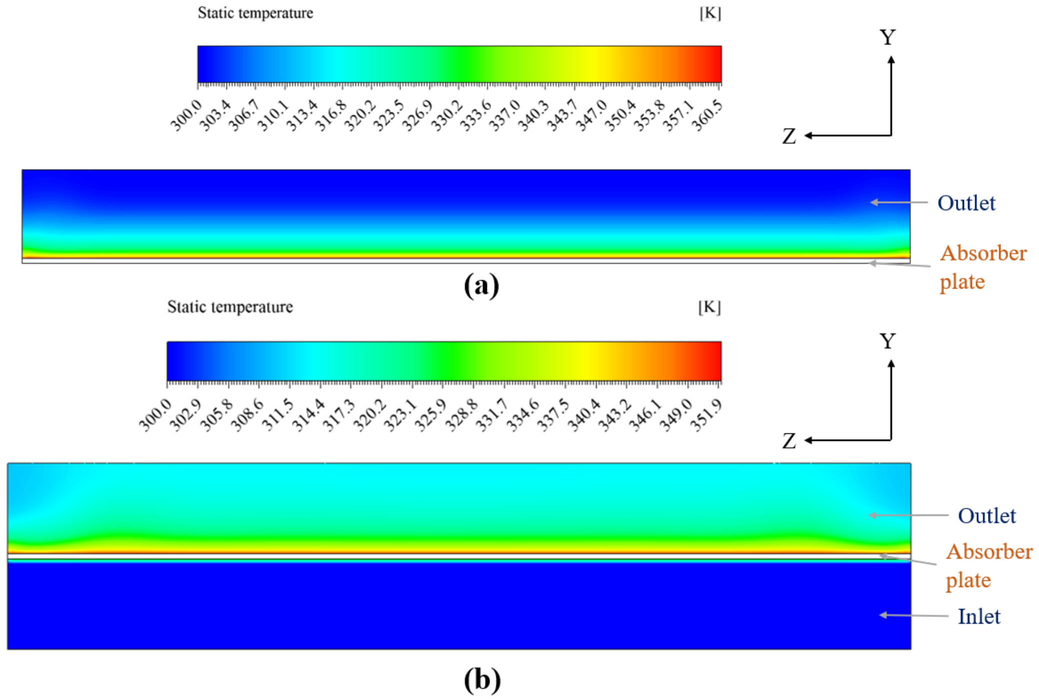

Fig. 9. Static temperature contours corresponding to Re of 7000 for (a) SPSAH and (b) DPSAH.

4.3. Performance comparison with previous research data

The present study analyzes the thermohydraulic performance of DPSAH over SPSAH. The maximum value of THPP is determined as 1.25 at *Re* of 19000. An attempt has been made to compare the THPP value with the previous studies, as presented in Tab. 4. The smooth DPSAH increases the THPP value by 10.4%, 15.2% and 1.6% over the discrete D-shaped ribs (Dutt et al. 2023), transverse wire ribs (Gupta, Solanki, and Saini 1997) and two truncated ribs (Sharma and Kalamkar 2017), respectively.

Tab. 4. Comparison of the results of this study with those of previous studies

References	Investigated geometry	$(Nu/Nu_s)_{max}$	$(f/f_s)_{max}$	THPP
Dutt et al. (2023)	Discrete D-shaped ribs	1.41	2.09	1.12
Gupta et al. (1997)	Transverse wire ribs	-	-	1.06
Sharma and Kalamkar (2017)	Two truncated ribs are placed with total truncation of 10% (10 mm) on one side	1.78	7.4	1.23
Present study	Smooth double pass solar air heater (DPSAH)	1.89	3.5	1.25

5. Conclusions

In this study, different turbulence models and thermohydraulic performance of a DPSAH are optimized for various values of *Re* from 3000 to 19000. Following is a summary of the major findings of the study:

- For the considered range of *Re*, the RNG k-ε turbulence model with enhanced wall treatment is found in close agreement to experimental results with MAPE of 2.6% for Nusselt number (*Nu*) and MAPE of 0.4% for friction factor (*f*).
- The standard k-ω model, SST- k-ω model, standard k-ε model and realizable k-ε model are also validated with experimental results of Nusselt number (*Nu*) with MAPE of 8.6%, 11%, 4.8% and 4.1%, respectively.
- Similarly, standard k-ω model, SST- k-ω model, standard k-ε model and realizable k-ε model are also validated with experimental results of friction factor (*f*) with MAPE of 0.8%, 2%, 2.1% and 3.9%, respectively.

- For the range of *Re*, the DPSAH enhanced the values of Nu/Nu_s from 1.13 to 1.89 and increased the values of f/f_s from 2.69 to 3.5 in comparison to SPSAH.
- The maximum thermohydraulic performance parameter (THPP) over the SPSAH was obtained as 1.25, which corresponds to *Re* of 19000.

6. Acknowledgement

The authors are grateful to the Ministry of Education (MoE), Government of India, for providing financial support in the form of fellowship for the research work. We also acknowledge the National Supercomputing Mission (NSM) for providing computing resources of 'PARAM Ganga' at IIT Roorkee, which is implemented by C-DAC and supported by the Ministry of Electronics and Information Technology (MeitY) and Department of Science and Technology (DST), Government of India.

7. References

Alam, T., Man H.K., 2017. Performance improvement of double-pass solar air heater – A state of art of review. Renew. Sust. Energ. Rev. 79, 779–793.

Bhatti M. S., Shah, M.S., 1987. Turbulent and transition flow convective heat transfer in ducts, in: Kakac, S., Shah, R.K., Aung, W. (Eds.), Handbook of single-phase convective heat transfer, Wiley., New York, pp. 32

Brown, G 2002. The history of the darcy-weisbach equation for pipe flow resistance. *Proceedings of the Environmental and Water Resources History*, United States, 3-7 November.

Dutt, N., Hedau, A.J., Kumar, A., Awasthi, M.K., 2023. Thermo-hydraulic performance of solar air heater having discrete D-shaped ribs as artificial roughness. Environ. Sci. Pollut. Res. 1, 1–22.

Gill, R. S., Singh, S., Singh, P.P., 2012. Low cost solar air heater. Energy Convers. Manag. 57, 131–142.

Gupta, D., Solanki, S.C., Saini, J. S., 1997. Thermohydraulic performance of solar air heaters with roughened absorber plates. Sol Energy. 61, 33–42.

Hernández, A.L., and Quiñonez, J.E., 2013. Analytical models of thermal performance of solar air heaters of double-parallel flow and double-pass counter flow. Renew. Energy. 55, 380–391.

Kabeel, A. E., Hamed, M.H., Omara, Z. M., Kandeal, A.W., 2017. Solar air heaters: Design configurations, improvement methods and applications – A detailed review. Renew. Sust. Energ. Rev. 70, 1189–1206.

Kareem, M. W., Habib, K., Sulaiman, S. A., 2013. Comparative study of single pass collector and double pass solar collector filled with porous media. J. Asian Sci. Res. 6, 445–455.

Kays W. M., Perkins, H. C., 1985. Forced convection, internal flow in ducts, in: Rohsenow, W.M., Hartnett, J.P., Ganic, E.N. (Eds.) Handbook of Heat Transfer Fundamentals, Second ed. Mac-Graw Hill, New York.

Kumar, A., Shinde, S.M., Gholap, A., Vyavahare, M.P., Gangarde, R., Mete, V.B., 2017. Performance of solar air heaters with corrugated absorber plate-A CFD approach. Int. J. Innov. Res. Adv. Stud. 4, 76–86.

Sharma, S.K., Kalamkar, V.R., 2017. Experimental and numerical investigation of forced convective heat transfer in solar air heater with thin ribs. Sol Energy. 147, 277–291.

ASHRAE Standard., 1986. Methods of testing to determine the thermal performance of solar collectors, in: Engen, B.W. (Eds.), American Society of Heating, Refrigerating and Air-Conditioning Engineers. Atlanta, pp. 1-42.

Webb, R. L., Eckert, R.G., 1972. Application of rough surfaces to heat exchanger design. Int. J. Heat Mass Transf. 15, 1647–1658.

Yadav, A.S., Bhagoria, J. L., 2013. Heat transfer and fluid flow analysis of solar air heater: A review of CFD approach. Renew. Sust. Energ. Rev. 23, 60–79.

IEA. 2021. Electricity Sector – Analysis - IEA. https://www.iea.org/reports/electricity-sector (May 15, 2023).